Deformation Analysis to Detect and Quantify Active Lesions in Three-Dimensional Medical Image Sequences

Jean-Philippe Thirion, Guillaume Calmon

▶ To cite this version:

HAL Id: inria-00615095

https://hal.inria.fr/inria-00615095

Submitted on 17 Aug 2011

Deformation Analysis to Detect and Quantify Active Lesions in Three-Dimensional Medical Image Sequences

Jean-Philippe Thirion* and Guillaume Calmon

Abstract—**Evaluating precisely the temporal variations of lesion volumes is very important for at least three types of practical applications: pharmaceutical trials, decision making for drug treatment or surgery, and patient follow-up. In this paper we present a volumetric analysis technique, combining precise rigid registration of three-dimensional (3-D) (volumetric) medical images, nonrigid deformation computation, and flow-field analysis. Our analysis technique has two outcomes: the detection of evolving lesions and the quantitative measurement of volume variations. The originality of our approach is that no precise segmentation of the lesion is needed but the approximative designation of a region of interest (ROI) which can be automated. We distinguish between tissue transformation (image intensity changes without deformation) and expansion or contraction effects reflecting a change of mass within the tissue. A real lesion is generally the combination of both effects. The method is tested with synthesized volumetric image sequences and applied, in a first attempt to quantify *in vivo* a mass effect, to the analysis of a real patient case with multiple sclerosis (MS).**

Index Terms—**Lesion, mass effect, motion field analysis, multiple sclerosis, 3-D deformable grid, 3-D image processing, stereology, volume measurement.**

I. INTRODUCTION

THE precise evaluation of lesion-volume variations along time is extremely important for the following reasons (see, for example, [20], [17]:

- for pharmaceutical research, to compare the effects of new drugs on different populations of patients;
- for clinical applications, to determine the exact time when a potentially invasive drug is to be given, or surgery is to be performed;
- for clinical follow up, to quantify the effects of the drug or surgery along time.

The main source of *in-vivo* information about lesion growth is volumetric medical imaging such as three-dimensional (3-D) magnetic resonance images (MRI). Classical techniques (see, for example [15] and [16]) consist in delineating the lesion in two volumetric images of the patient at two different time points t_1 and t_2 which gives two volumes $V_1 = V(t_1)$ and $V_2 = V(t_2)$ to be compared. The volume variation $\Delta V = V_2 - V_1$ is an index of the lesion evolution.

This measurement is difficult to perform for at least two reasons: the first is delineating in three dimensions and the second is delineation errors. Because hundreds or thousands of voxels are to be considered, (semi-) automatic segmentation tools are highly desirable for routine applications because they can offer an automation of tedious and repetitive tasks, as well as providing objective measurements. Among possible automatic segmentation tools are the mathematical morphological operators (erosion, dilation, connected components analysis, etc., or the 3-D extension of deformable models (3-D snakes, see [3]). In most practical cases, however, the *a priori* medical knowledge of the physician is indispensabl. Most of these methods incorporate an interactive initialization and a final interactive adjustment tool. Generally also, the accuracy of the delineation is not subvoxel, hence, the uncertainty σ_V on the total volume measurement can be higher than the volume variation itself $(2\sigma_V > \Delta V)$.

The main idea in this paper is to use an analysis method based on a volumetric deformation field to first detect the active lesions and then to evaluate their volume variations. In particular, our volume-variation measurement necessitates as input only the designation of a region of interest (ROI) surrounding the lesion (for example a sphere) or, when it is possible, a segmentation of the lesion which is not requested to be subvoxel. Because we use a precise 3-D rigid registration method, this ROI designation or rough segmentation needs to be performed only in (one) of the two volumetric images or one image of the time sequence to be analyzed, rather than at each time frame. Rather than a single value ΔV of volume variation, our method provides a kind of signature, or profile, associated to the lesion growth, from which we propose to quantify different effects that we call the tissue transformation and the (tissue deformation).

First we give a general description of the method and a definition of the tissue transformation and deformation effects. Then we concentrate on the description of the deformation-field analysis, which is the main contribution of our paper. Mainly, we have developed a new method of analysis based on the integration of the deformation field according to concentric shapes: either concentric spheres or shapes described as a set of
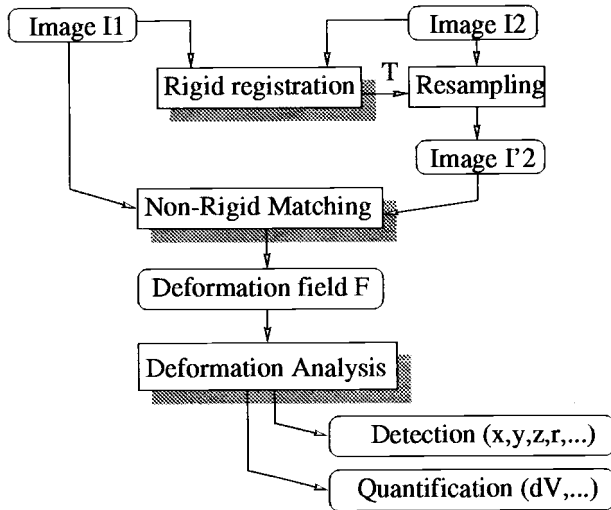
Fig. 1.   The general principle of the method.

isocontours. We present experimental results with synthesized images to evaluate the performance and test the robustness of our method. Last, we apply our method to sequences of volumetric images of a patient with multiple sclerosis (MS), to evidence and quantify a tissue deformation or mass effect at the level of the plaques: an effect which, to our knowledge, has never been quantified *in vivo* before.

II. GENERAL DESCRIPTION

The method consists of four steps (see also Fig. 1).
1) The 3-D rigid registration of the two successive images.
2) The computation of the deformation field between the two registered images.
3) The detection of evolving lesions.
4) The vector field analysis at the level of each detected lesion to quantify the volume variation.

The most original part of the present work are the last two steps: the vector field analysis for both the detection and the quantification of evolving lesions.

For the first step, which is the computation of a rigid transformation between two volumetric images I_1 and I_2, we use the automatic rigid matching method based on extremal points described in [18]. The accuracy of this method has been evaluated in [13] and is of the order of $1/10$th of a voxel, assuming that the object which is scanned is really rigid. To fulfill this hypothesis, even when some part of the object are deformed (such as places containing lesions), the matching method is based on feature points extraction and outlier features are automatically discarded in the computation of the final transform. We then resample one of the two images (let say I_2) into I_2' to make it exactly superposable to I_1 except, of course, for the regions of the brain which have changed between the two acquisitions (that is, mainly the lesions). Note also that, for simplicity reasons, we are considering isotropic volumetric images. In our experiments we always resample the data into isotropic volumes before processing them. Typically, a $0.94 \times 0.94 \times 3.0$-mm MR image is resampled into 0.94 mm^3 before processing.

We then compute the nonrigid deformation between I_1 and I_2' using the nonrigid matching method described in [19]. It is a 3-D deformable grid technique which is very close to optical flow when small deformations are considered. The result is a dense (i.e., not restricted to contour points) deformation field f, represented by a 3-D array of displacement vectors, one for each voxel in the image I_1. As in many nonrigid matching methods, the result of the motion field estimation depends on a parameter σ which is a balance between the regularity of the deformation field and the similarity between $I_2'' = f^{-1}(I_2')$ and I_1. It is very unlikely that this parameter σ, which is inherent to any nonrigid matching technique, can be eliminated. For the snakes methods [see [11]] it is the balance between internal forces (regularity) and external forces (similarity).

This parameter σ has some influence on the volume-variation analysis. It can be interpreted to some extent as a blurring of the real deformation field, equivalent to a convolution with the Gaussian function $e^{-r^2/2\sigma^2}$ of the vector field (see [2]). This value σ is explicitly defined in the nonrigid matching method that we are using (see [19]).

The next sections describe in detail the detection of evolving lesions and the quantification of volume variation. First we must define precisely the effects that we want to measure.

III. TISSUE DEFORMATION AND TRANSFORMATION

We distinguish between two different models of lesion growth, real cases being generally a mix of these effects. Our model is crude with respect to many other works existing in the medical domain and concerning the biological aspects of lesion growth (see, for example, [21] and [5]). In particular, we consider explicitly neither the elastic properties of the brain tissues (see [6]), nor the dynamic aspect of malignant cells growth, but only two fixed time frames, with no (or very few) biological *a priori* knowledge. We will see, however, that even with crude assumptions, solving the problem is not an easy task.

What changes can be observed in a medical image of a lesion? A lesion can be the inclusion or destruction of material within the tissue, or a localized change of the tissue properties, or a complex combination of those cases, which might or might not have the same appearance in MR images. Basically, we distinguish between deformation and transformation.

A. Tissue Deformation

Some lesions can be observed by way of a large deformation of the tissues (mass effect) without image intensity changes. Additional material is entering the tissue, but it may happen that the grey-level value representing the tissue in the MRI is unchanged, mainly because their proton density is the same. Hence, the only visible effect in that case is an expansion, contraction, or deformation of the tissue, which can be perceived only due to textural information. We call this effect (diffuse) deformation. But it also can be the addition of new untextured material in the central part of the lesion, which translates into two effects: the growing of a central spot (the lesion) and the displacement of the surrounding tissues (the deformation). We call this model central deformation.
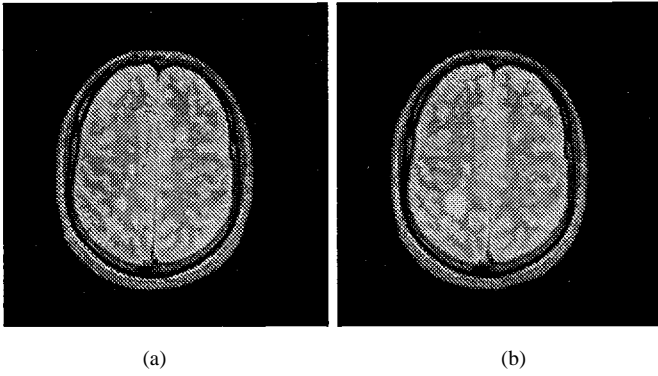
(a)   (b)

Fig. 2. Two registered slices of a patient with MS, with a two-months interval (T_2-weighted first echo MRI).

B. Tissue Transformation

A lesion also can be detected by a change in intensity without any displacement of the tissues. The molecular structure of the tissue is changing in place: the tissue itself is not displaced. This type of lesion is, of course, much easier to delineate than in the previous case. The lesion volume is the area of the MR image where the tissue has a different composition and, therefore, a different gray value. It is a known phenomenon for the plaques in T_2-weighted MR images of MS, which corresponds to demyelination of the axons and then glyosis. Most of the classical lesion-measurement methods are based on this model and are using segmentation tools exclusively.

C. Defining Volume-Variation Measurements

Of course, real lesions are always a complex combination of these effects and giving a clear definition the lesion volume or lesion growth is very difficult. If central deformation and tissue transformation might present the same appearance in the MRI within the lesion itself (i.e., translates into a contrasted central region), they have different influences on the nearest surrounding tissues. This leads to the idea of studying a lesion-evolution profile $\Delta V(r)$. A curve representing the volume-variation coefficient ΔV as a function of the distance r to the approximate center of the lesion P and up to a limiting bounding radius R. The sphere (P, R) defines an ROI centered on the lesion. By studying the profile $\Delta V(r)$ outside the lesion (but inside the ROI), we might be able to distinguish deformation ($\Delta V(r) = \Delta V$ and $\|f\| \approx 1/r^2$ outside the lesion) from transformation ($\Delta V(r) = 0$ and $\|f\| = 0$ outside the lesion) where f is the vector field corresponding to the displacement of tissues.

D. An Ideal Mathematical Solution

Ideally, if we define a virtually closed surface S in the image space enclosing a region $\mathcal{R}$ of volume V we can study the flux of tissues through S, represented by the vector field f produced by the nonrigid matching step. Intuitively, the summation of all that goes out minus the summation of all that enters is equal to the volume variation, which is a simplified version of the Ostrogradsky theorem which states that the integral over a closed surface of the flux of a vector field is equal to the integral over the encompassed volume of the divergence of

the vector field. In practice, different factors prevent us from directly using this mathematically well-defined technique. We list now some of these problems with some possible (partial) solutions.

- The vector field f produced by an intensity-based non-rigid matching is equally sensitive to a deformation or a simple intensity change (transformation).

    We can study precisely and separately ideal measurement models for tissue deformation and transformation, test these models on synthetic data, and compare the profiles with those obtained with real data.

- The estimated vector field is inevitably blurred by a regularity parameter σ.

    We can quantify the effect of this blurring on ideal models and measure it in the synthesized models to extrapolate it to real data.

- A lesion can have a shape much more complicated than a sphere.

    We can study a family of embedded closed surface $\{S_i, i \in [1 \cdots m]\}$ encompassing regions $\mathcal{R}_i$ of volume V_i, ranging in size from the approximate center point of the lesion to the complete ROI. It defines a profile of the lesion variation $\{\Delta V_i, i \in [1 \cdots m]\}$. If the lesion can be approximately segmented, we can use a family of embedded surfaces whose shapes are much closer to the segmented lesion surface than spherical shells.

- f is not a continuous field, but is sampled for a regular 3-D grid (the voxels). It is unclear how to integrate a discrete flow field over a sampled closed surface.

    We develop in this paper a stochastic method to integrate the volume variation from a discrete deformation field.

- The displacement of surrounding tissues induced by a lesion evolution decreases in $(1/r^2)$ outside the lesion, and the vector field evaluation is inherently corrupted by measurement errors and discretization, hence, the evaluated flow becomes meaningless very rapidly when we get farther from the lesion. In addition, there might be several active lesions, as in the case of MS disease.

    High-frequency noise is eliminated by the regularization of the vector field, but we must keep close to the lesion boundary for meaningful measurements.

- Different pathologies exist, corresponding to different models of lesions.

    The usefulness of the discrimination power of each measurement has to be proved for each specific type of disease through *in vitro* studies and through clinical validations (coherence of the measurements along time, coherence with traditional clinical tests based on external symptoms, coherence with histology, etc.

As we can see, the problem of defining and measuring a precise lesion volume variation is much more complex than simply counting voxels. But even if no complete mathematical formulation is at hand, the precise quantification and its impact on the development of new drugs is too important to simply abandon the effort when things become difficult. For example, in the case of MS, there are hundred thousands of patients

throughout the world and the cost of therapy based on β interferon is very high (today, approximately \$10 000 per year per patient). In the following, we describe the solutions that we have explored to detect and quantify the evolution of such lesions.

IV. DETECTING EVOLVING LESIONS

In this section, first we present traditional methods based on segmentation to analyze lesion evolutions and then a more recent work based on the temporal analysis of the intensity signal ([8]). Finally, we present our contribution, which is based on the evaluation and analysis of deformation fields and present an original method which evaluate volume variation through the integration of the deformation field in concentric shapes, which can be concentric spheres or embedded isosurfaces.

A. Segmentation

Detecting lesions in medical images is traditionally performed by segmentation and, therefore, relies on the local analysis of the intensity or texture in static images. Unfortunately, the intensity is generally not specific enough to automatically characterize a lesion and, in most cases, several modalities must be used to image the same brain. By combining those different images it is sometime possible to characterize the lesions in a more robust way, for example, by a component-classification method (see [7] and [4]). Once the lesions are characterized in each time frame, it is possible to analyze the whole sequence of segmented images as a four-dimensional (4-D) image (3-D + time) and extract and analyze the lesions as 4-D connected components (see [10] and [12]). On the one hand, this allows us to extract static as well as dynamic lesions. On the other hand, the motion information is not taken into account in the detection itself.

In the case of MS, there are several serious drawbacks in using segmentation methods. In T_2-weighted MR images, the boundary of an MS plaque is fuzzy and sometimes surrounded by a halo. Hence, it is very difficult to segment. In [10], this problem is partially overcome due to masking. In addition, thresholding and connected component analysis tools are very unstable operators. For example, an active plaque can merge with a neighboring passive plaque during the expansion. The estimated volume is suddenly and artificially increased due to the capture of the passive plaque or of another brain structure. This prevents us from studying precisely and automatically the evolution of individual plaques with segmentation, although it might be possible to obtain some global measurements. Even manually, segmentation is very difficult to perform in many cases. The final drawback of segmentation is that it totally ignores the mass effect (i.e., the effects on surrounding tissues).

B. Segmentation Based on Intensity Changes

A different approach is to consider a set of successive volumetric images of the same subject as being a temporal sequence (see Fig. 3).

A simple way to use the temporal domain is to consider the difference between two consecutive volumetric images (see

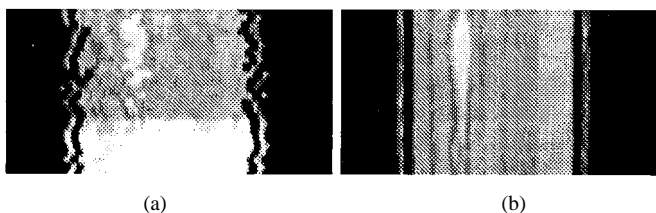

(a)   (b)

Fig. 3. Evolution of a lesion through time. The horizontal axis is a cross section of a 2-D image (itself extracted from a volumetric image). The vertical axis is time (20 different volumetric acquisitions for this subject). (a) The temporal sequence without volumetric image matching. (b) The evolution after image matching and 3-D resampling: the evolving lesion appears as a spindle shape. This sequence corresponds to a horizontal cross-section through the evolving lesion presented Fig. 2.
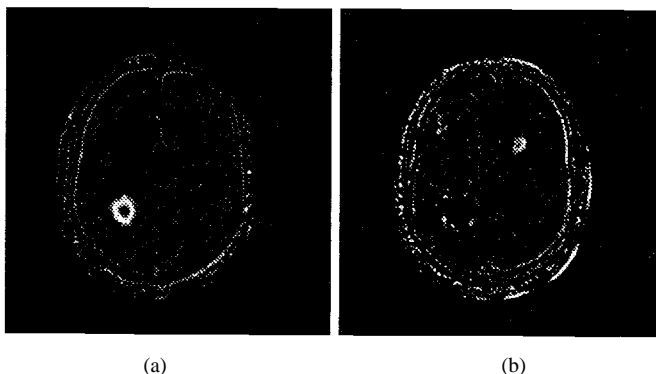

(a)   (b)

Fig. 4. (a) Subtraction image: the growing lesion appears as a white annulus. (b) The subtraction image [same image as (a)] is inverted and a small shrinking lesion can be seen (upper right).

Fig. 4). When a lesion is characterized by a hypersignal, that is, with an intensity locally larger than the intensity of the surrounding tissues, then a growing lesion appears as a white annulus in the difference of two consecutive images, and a shrinking lesion appears as a black annulus. Provided with an almost perfect registration of the images, the annulus can be isolated more easily in a difference image than a lesion in a single static image (compare Figs. 2 and 4).

In [8] the intensity profile of the whole sequence of registered volumetric images is analyzed individually for each voxel position to characterize evolving regions. In this last work, no deformation due to lesions is considered, which might induce interpretation problems if there is indeed a displacement of the tissues.

If we are looking carefully at Fig. 3 (see also Fig. 2), we can perceive tissue displacements: the white spindle is the evolving (growing then shrinking) lesion. The first dark layer around the spindle is gray matter, followed by a lighter layer which is white matter, etc. As we can see, the widths of these layers remain fairly constant and the layers themselves are displaced by the evolving lesion. It has no visible effects farther from the lesion because, in 3-D, displacements due to mass effects are decreasing very rapidly (in $1/r^2$). Such spatial displacement is even more apparent in Fig. 2(b) and [8, p. 474] (same patient but different lesion).

C. Flow-Field Analysis

We have developed a different way to characterize evolving lesions than simply analyzing image intensity evolutions.
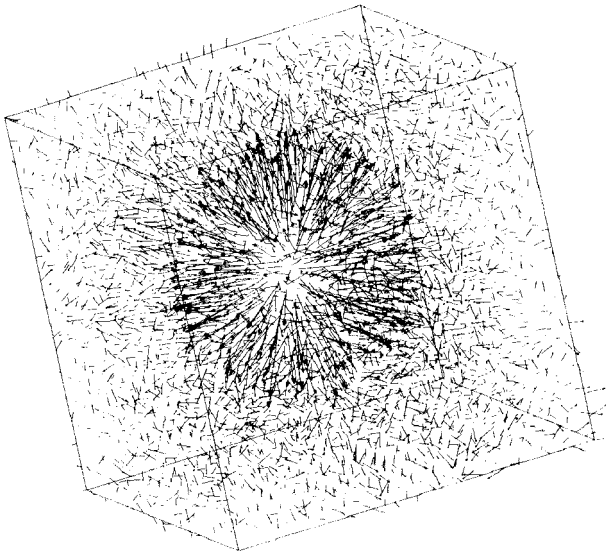
Fig. 5. The 3-D deformation field measured between the two volumetric MRI's of the same patient, at the level of the lesion (this lesion is visible in Fig. 2).

We analyze the deformation field f computed between two consecutive images I_1 and I_2 (see Fig. 5). f is represented by a discrete function $f(x, y, z)$ where f: (u, v, w) is a 3-D displacement vector defined at each voxel (x, y, z) of I_1. More precisely, $f(P)$ being the position in I_2 corresponding to a point P: (x, y, z) in I_1, we have

$$f(P): \begin{pmatrix} x + u(x, y, z) \\ y + v(x, y, z) \\ z + w(x, y, z) \end{pmatrix}. \tag{1}$$

We are interested in places presenting large deformations ($\|f\|$ large) and, in addition, because MS plaques have generally a rather spherical shape, places where the divergence $\operatorname{div}(f) = \partial u/\partial x + \partial v/\partial y + \partial w/\partial z$ is large (see Fig. 6). In some places $\|f\|$ can be large and $|\operatorname{div}(f)|$ low (in case of a translation, for example) or $|\operatorname{div}(f)|$ can be high and $\|f\|$ low (in noisy regions), but as the feature high magnitude high divergence is more specific to evolving lesions, we have tested successfully the following operator $\|f\|\operatorname{div}(f)$. Besides, the sign of $\operatorname{div}(f)$ characterizes growing lesions from shrinking lesions. This operator makes active lesions very easy to detect (see Fig. 6). In addition, in the case of MS plaques we can use a mask representing the white matter in the brain, because most of the MS plaques appear in the white matter. We use thresholding and connected component analysis to finally extract automatically the centers and the approximative radii of the active lesions.

V. MEASURING THE VOLUME VARIATION PROFILE

For now, we assume that the approximate center P and radius R of an active lesion is determined and that we are looking for a precise volume-variation measure. We assume also that there is a single lesion present in the defined ROI. This assumption might restrain the applicability of the method for some pathologies.
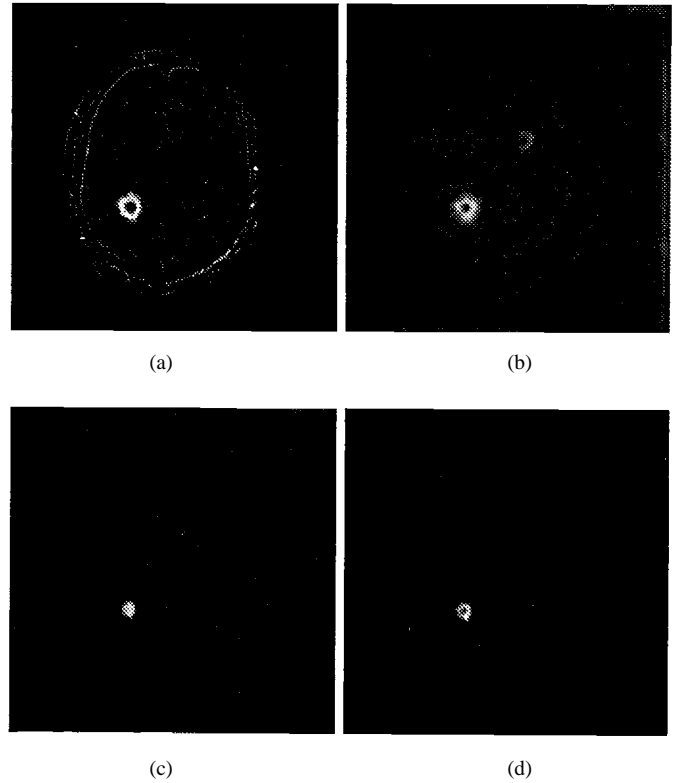

Fig. 6. (a) Difference of intensity. (b) Vector field norm $\|f\|$. (c) Divergence $\operatorname{div}(f)$. (d) $\|f\|\operatorname{div}(f)$. Each step corresponds to an image easier to segment automatically.

We describe now the method that we have applied in our experiments, which is based on the integration of the vector field for a set of concentric shapes, either spherical or defined by a set of isocontours.

A. The Method of Concentric Spheres

In this section we consider a family of n spheres S_i of increasing radii $\{(P, r_i), r_i \in [0 \cdots R]\}$ where R is set by the user to entirely encompass the lesion and some of the surrounding tissues (but, hopefully, no other lesions). The aim of the concentric spheres is to obtain a volume-variation profile and to deduce from it the volume variation, without having to segment the lesion.

1) Integrating the Divergence: A first idea is to compute the integral of the divergence within each sphere S_i, or the integral of the flux on the surface of the sphere which is theoretically equivalent (n is the normal to the sphere)

$$\Delta V(r_i) = \int_{S_i} f \cdot n \, dS = \int_{V_i} \operatorname{div}(f) \, dV. \tag{2}$$

For a growing lesion $\Delta V(r_i)$ must increase when i is increased until the lesion is entirely included into (P, r_i). At that point, $\Delta V(r_i)$ remains constant (for the deformation model only, not for pure transformation). Up to now, however, we did not get good results in practice with such methods, probably because the noise in the vector field is amplified in the computation of the divergence which necessitates a differentiation.

2) A Stochastic Computation: We have then switched to a stochastic method to evaluate the volume variation which is the following.

Assume a shape S, for example, a sphere, a cube, or any shape defined by a closed oriented surface in image I_2. Assume also a regular grid G [see Fig. 7(a)]. The number of grid nodes times the volume of a single voxel $V(\text{voxel})$ is an approximation of the total volume $V(S)$ of S, which tends to the exact value when the grid gets thinner. This method is close to stereological methods which are used to quantify the volumes of static lesions (see [14]). Similarly, the number of nodes of the regular grid G within the deformed shape $f^{-1}(S)$ gives an approximation of $V(f^{-1}(S))$ [Fig. 7(c)].

As $f^{-1}(S)$ is the image in I_1 of the shape S in $I_2, \Delta V(S) = V(S) - V(f^{-1}(S))$ is the volume variation between I_1 and I_2 of the shape represented by S in I_2 (or by $f^{-1}(S)$ in I_1).

We could compute $\Delta V(S)$ by computing stochastically $V(S)$ and $V(f^{-1}(S))$, which would necessitate the computation of the deformed shape $f^{-1}(S)$. However, we note that computing the number of nodes of G within the deformed shape $f^{-1}(S)$ is equivalent to computing the number of nodes of the deformed grid $f(G)$ within the original shape S [Fig. 7(b)], which is computationally much easier because the deformation f is sampled for each node of G and there is no need to compute the deformed shape $f^{-1}(S)$.

The method that we propose is fairly simple, but counter-intuitive. Compute the number $N_S(G)$ of nodes of G within S and the number $N_S(f(G))$ of nodes of $f(G)$ also within S. The volume variation $\Delta V(S)$ for the shape S in I_2 is approximately $N_S(G) - N_S(f(G))$. This approximation tends to the exact value when the grid gets thinner. If the volume variation is requested for a regular shape within I_1 instead of within I_2, it suffices to use the same method with the inverted transformation f^{-1} obtained, for example, by the exchange of I_1 and I_2 within the nonrigid matching algorithm.

3) Practical Computation of the Profile: Suppose now that we have a family of embedded shapes $S_i, i \in [0 \cdots m]$ such as, for example, a family of spheres (P, r_i) with increasing radii r_i. We propose an optimal algorithm (i.e., with a linear complexity) to compute the volume-variation profile. Suppose that we have defined a ROI (P, R) containing n grid nodes of G.

- We define two arrays of numbers $\{M_i^G\}$ and $\{M_i^{f(G)}\}$, initialized to zero.
- For each node P_j: (x, y, z) of G (out of the n nodes), we determine the index i of the shell corresponding to the spheres (P, r_i) and (P, r_{i+1}) which contains P_j (respectively, $f(P_j)$). i can be obtained in constant time with the distance $d(P_j, P)$ and a lookup table. For each P_j we increment the corresponding bucket M_i^G (respectively, $M_i^{f(G)}$).
- Once the arrays $\{M_i^G\}$ and $\{M_i^{f(G)}\}$ are computed, we compute incrementally the arrays $N_i^G = \Sigma_{k=0}^{i-1} M_k^G$ and $N_i^{f(G)} = \Sigma_{k=0}^{i-1} M_k^{f(G)}$
- At last, we compute the volume-variation profile $\Delta V_i = (N_i^G - N_i^{f(G)}) \times V(\text{voxel})$
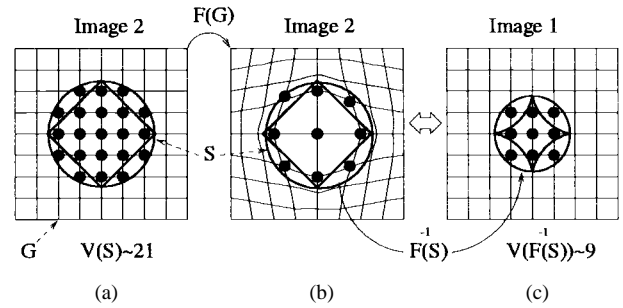

Fig. 7. Stochastic computation of the volume variation. The main idea is that the stochastic computation of the volume of a shape $f^{-1}(S)$ with a regular grid G (a) is equivalent to the stochastic computation of S with a deformed grid $f(G)$ (b).
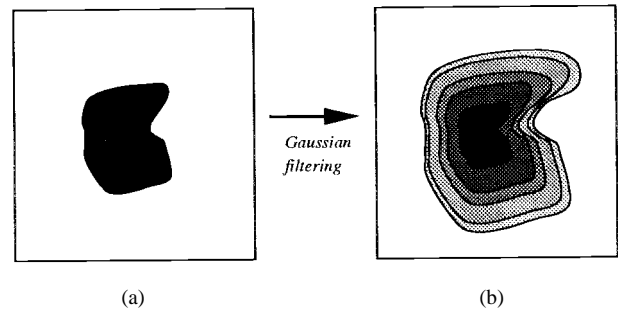

Fig. 8. Automatic computation of embedded surfaces from an approximative segmentation of the lesion.

The computational complexity of the arrays $\{M_i^G, i \in [0 \cdots m-1]\}$ and $\{M_i^{f(G)}, i \in [0 \cdots m-1]\}$ is $O(n)$, as for the derivation of $\{N_i^G\}$ and $\{N_i^{f(G)}\}$ from $\{M_i^G\}$ and $\{M_i^{f(G)}\}$, hence, the whole computation of the volume-variation profile $\{\Delta V_i, i \in [0 \cdots m-1]\}$ is linear $(O(n))$.

We shall note that this computation can also be performed with random positions P_j throughout the ROI instead of with the nodes of a regular grid G.

4) Computation of a Single Value of Volume Variation: For the deformation model, ΔV_i must remain constant and equal to the searched ΔV as soon as r_i is larger than the maximal extent of the lesion. However, because of the noise, ΔV_i moves with a Brownian motion around the true ΔV (each new error increments or decrements the estimated value randomly), which means in practice that ΔV_i oscillates around ΔV with larger and larger amplitudes when i is increased. To avoid this phenomenon, we remove from the computation the effect of very small displacements (when $\|f\| < \text{threshold}$ we impose $f = 0$). With this constraint, the noise is reduced but ΔV_i tends artificially to zero when r_i becomes large, even for the deformation model, which is one of the reason which prevent us from directly using the volume profile to distinguish between transformation and deformation.

In order to get a single value of volume variation, we compute the maximal value $\Delta \overline{V}$ of $\{\Delta V_i, i \in [0 \cdots m-1]\}$, which approximates the real ΔV. We have extensively validated this method with synthesized data, which constitutes an important part of the present paper.

B. Computing ΔV_i with Isointensity Surfaces

The advantage of using concentric spheres is that it doesn't necessitate any kind of segmentation and hence can be applied to invisible lesions (invisible meaning undetectable in a single frame). However, it can be improved seriously if we can take into account an approximate shape of the lesion by replacing concentric spheres by concentric shapes closer to the actual shape of the lesion.

If the lesion is sufficiently contrasted, it can be segmented as a set of labeled voxels $\mathcal{R}$ in image I_2. In the previous algorithm we have replaced the spheres (P, r_i) with a family of embedded closed surfaces $S_i, i \in [0 \cdots m]$. A simple way to obtain this family of surfaces is to consider a digital volumetric image $I_{\mathcal{R}}$ where the voxels are labeled zero if they are outside $\mathcal{R}$, or one if they are inside. We then blur this image with a Gaussian filter. The isointensity surfaces for a set of increasing intensity constants $\{C_i, i \in [0 \cdots m], C_i \in [0, 1]\}$ have the requested properties (closed and embedded) and, furthermore, the intensity $I(P_j)$ of $I_{\mathcal{R}}$ at a point P_j directly gives the index i of the shell $[S_i, S_{i+1}]$, which contains P_j. Another equivalent solution is to precompute a 3-D distance map from $\mathcal{R}$ using, for example, the chamfer distance (see [1]). The rest of the algorithm is exactly similar to the case of the embedded spheres and therefore the whole algorithm still has a linear ($O(n)$) complexity (a few seconds of computation on a workstation).

The segmentation of $\mathcal{R}$ should be distinguished from the precise segmentation used to evaluate the volume variation in traditional methods. It can be much less precise (because it is then blurred) and, in addition, it must be performed only in one of the two images. If the lesion is well contrasted, using shells around a segmented lesion rather than simple spheres gives more reliable results because of the fast decrease ($1/r^2$) of the deformation magnitude. Of course, a better segmentation leads to a better deformation analysis. We have verified this assumption with synthetic data.

VI. Synthetic Experiments

A. Tissue Transformation

We suppose (see Fig. 9) that the lesion evolution is simply a change of intensity without tissue displacement. Another assumption is that the image intensity saturates at the level of the lesion, that is, textural information is lost in those regions.

To produce a synthetic lesion, we have measured the average intensity of plaques in a real MRI, selected a region where the white matter of the brain is homogeneous, and implanted spherical synthetic lesions of known radii in it (see Fig. 10). The boundaries of the synthetic lesions are blurred to give a realistic appearance to the false MS plaque. In this model, the deformation field measured by our method is strictly due to intensity changes and not to tissue motion. We have compared the volume variation obtained by our deformation-field analysis method based on embedded spheres, embedded isosurfaces, and also with segmentation (see Table I). The segmentation used is based on thresholding
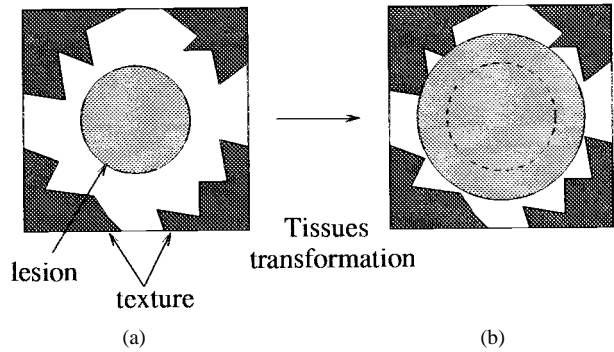

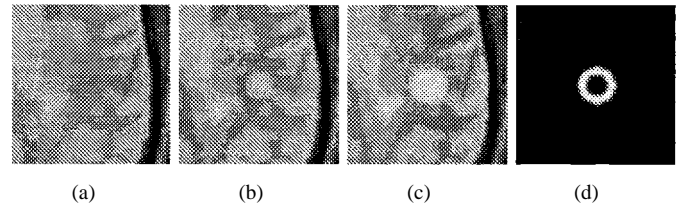Fig. 9. Tissue transformation: intensity change without tissue displacement.

Fig. 10. (a) Original image. (b) Synthesized lesion with radius R_1 (I_1). (c) Synthesized lesion with radius R_2 (I_2). (d) Subtraction $I_2 - I_1$.

TABLE I
EXPERIMENTS FOR INFLAMMATION: REAL VOLUME VARIATIONS (ΔV_{th}), SPHERES METHOD (ΔV_{sphere}), ISO-SURFACES METHOD (ΔV_{iso}), AND SEGMENTATION (ΔV_{seg}).

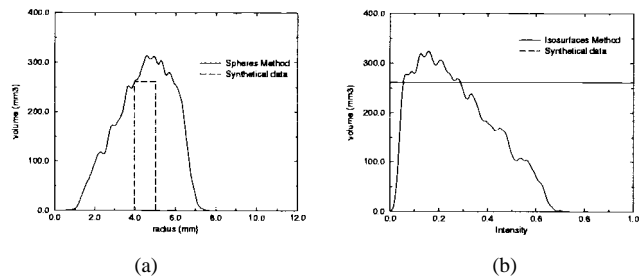| R_1	R_2	ΔV_{th}	ΔV_{sphere}	ΔV_{iso}	ΔV_{seg}
0	3.97	262	139	227	214
3.97	5	262	295	333	270
5	6.30	524	623	679	597
6.30	7.21	524	581	643	610
7.21	6.30	−524	−579	−642	−610
6.30	5	−524	−624	−681	−597
5	3.97	−262	−294	−336x	−270
3.97	0	−262	−176	−268	−214

Fig. 11. Profile of ΔV_i for tissue transformation: (a) with embedded spheres and (b) with isosurfaces .

and connected component analysis within an ROI defined by the user.

The profile ΔV_i for the sphere and for the isosurface method is presented in Fig. 11. Note that ΔV_i, which should be zero outside $[R_1, R_2]$, is in fact nonzero because of the regularization of the vector field. The measure which is finally retained is the maximum of ΔV_i, which in that case is a slight overestimation of the real value ΔV. Segmentation seems to perform slightly better than deformation-field analysis in that case (see Table I).
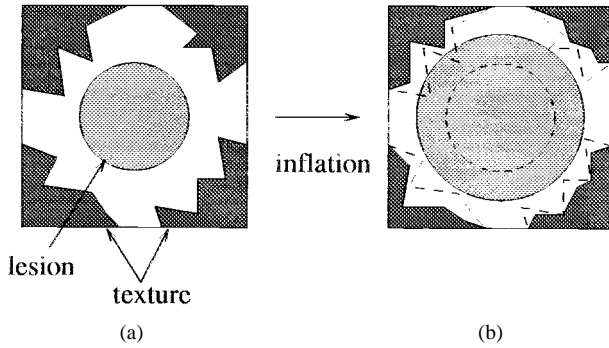
(a)

(b)

Fig. 12. Central deformation: addition of new material in the center of the lesion. The dashed lines in (b) represent the earlier positions of the lesion and textured tissues.

B. Mathematical Model of the Expansion Field

We now suppose that the lesion is growing in a limited spherical region of radius R_{lesion}, which means that inside this region the Jacobian determinant J of the deformation field f is larger than one. We suppose also that the surrounding tissues are incompressible, which is reasonable for the brain,[1] hence, the Jacobian determinant is one outside the lesion ($J = 1$). With this model, the expression of the synthetic deformation field is

$$f(x,y,z) = \left|\begin{array}{ll} (\sqrt[3]{J} - 1) \cdot r \cdot \boldsymbol{n}, & \text{if } r < R_{\text{lesion}} \\ (\sqrt[3]{(J-1)R_{\text{lesion}}^3 + r^3} - r) \cdot \boldsymbol{n}, & \text{if } r > R_{\text{lesion}} \end{array}\right. \tag{3}$$

The theoretical volume variation is then

$$(J-1)\tfrac{4}{3}\pi R_{\text{lesion}}^3. \tag{4}$$

The invert field (contraction) can be computed from this expression by replacing J with $1/J$ and R_{lesion} with $\sqrt[3]{J}R_{\text{lesion}}$. This computation is valid only in dimension three. The norm of the vector field $\|f\|$ is mathematically equivalent to $1/r^2$ outside $\sqrt[3]{J}R_{\text{lesion}}$. It should be noticed that in a two-dimensional (2-D) world, this field would only decrease in $1/r$, which can be counterintuitive when looking at a 2-D slice of a volumetric image. We must also remember that we choose to keep the Jacobian constant inside the lesion, but in real cases, the Jacobian could have a complicated profile $J(r)$ with respect to r and can be specific to each pathology.

C. Central Deformation

Here we suppose that the lesion evolution is the addition of untextured extra material to the disk of the lesion (see Fig. 12), therefore, in contrast to tissue transformation, the lesion is pushing the surrounding tissues.

To generate synthetic data we have inlayed a synthetic lesion in the first image (central spot of radius R_{lesion}), computed a synthetic deformation field with a known Jacobian within

[1] In the brain, the ventricles can compensate for volume variations induced by tumors or lesions, except when they are totally compressed or when the ducts are obstructed. As long as they can compensate, there is no increase of the intracranial pressure and, therefore, the compression of the brain tissues is fairly reduced. For preliminary works about the study of the biomechanical properties of the brain, one can refer too [9].
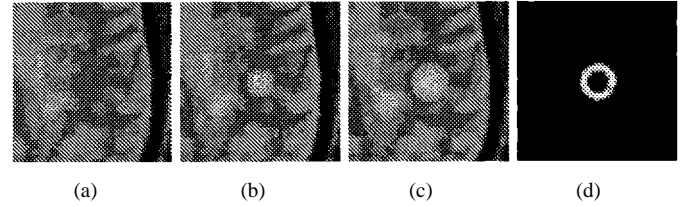

(a)   (b)   (c)   (d)

Fig. 13. (a) Original image. (b) Synthesized central spot (I_1). (c) Synthesized deformation is applied (I_2). (d) Subtraction $I_2 - I_1$.

TABLE II
SYNTHETIC EXPERIMENTS FOR CENTRAL DEFORMATION

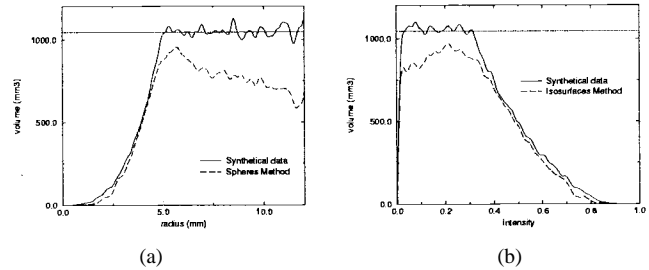| Jacobian	$\Delta(v)_{\text{th}}$	$\Delta(v)_{\text{sphere}}$	$\Delta(v)_{\text{iso}}$	$\Delta(v)_{\text{seg}}$
0.5	−262	−253	−239	−258
1.5	262	267	255	200
2	524	499	485	410
3	1047	989	974	872

(a)   (b)

Fig. 14. Profile of ΔV_i for central deformation: (a) embedded spheres method and (b) isosurfaces method. The upper curves are obtained with the synthetic deformation field and the lower curves with the retrieved deformation field and show a slight underestimation.

R_{lesion}, and, finally, applied this field to the first image with a resampling algorithm (see Fig. 13). In the difference image we note a small motion at the boundary of the brain due to the expansion. This is the only noticeable visible difference with the case of the tissue transformation (compare Figs. 10 and 13).

Table II presents experimental results comparing real and measured variations with embedded spheres, embedded isosurfaces, and segmentation. The segmentation underestimates the volume variation because the synthetic lesion is fuzzy and the intensity of its boundary is very similar to the one of the underlying image. In that case, the deformation-field method gives slightly better results than segmentation. Fig. 14 presents an example of measured profile.

D. Diffuse Deformation

In this last case, we apply a synthetic deformation field in a region of the image which does not present a particular intensity (see Fig. 15). No segmentation method can be applied at all: the lesion is invisible, even in the subtraction image. Only a slight displacement at the boundary of the brain can be observed (see Fig. 16). This small shift is the only evidence of an deformation of the tissue which, as we can see, can be partially retrieved thanks to the motion field analysis.

Table III shows that the measurements with the deformation-field techniques, although underestimating
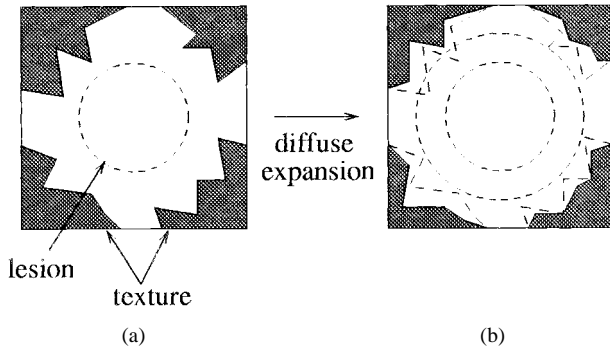
Fig. 15. Diffuse deformation: deformation of the tissues without intensity changes.
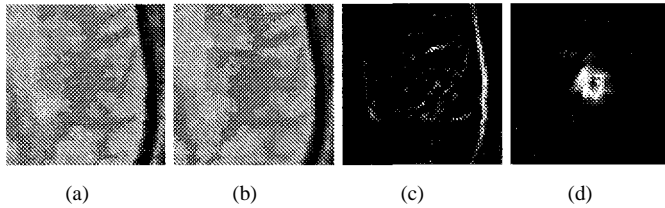

Fig. 16. (a) Original image (I_1). (b) Synthesized deformation (I_2). (c) Subtraction $I_2 - I_1$. (d) A detection of the lesion is possible thanks to the operator $\|f\| \operatorname{div}(f)$.

TABLE III
SYNTHETIC EXPERIMENTS FOR DIFFUSE DEFORMATION

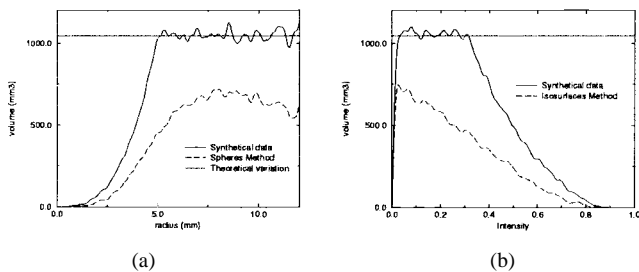| Jacobean	$\Delta(v)_{\mathrm{th}}$	$\Delta(v)_{\mathrm{sphere}}$	$\Delta(v)_{\mathrm{iso}}$	$\Delta(v)_{\mathrm{seg}}$
0.5	−262	−84	−63	0
1.5	262	148	198	0
2	524	329	327	0
3	1047	711	714	0

Fig. 17. Profile of ΔV_i for diffuse deformation. (a) Spheres. (b) Isosurfaces.

the real volume variation, are interesting indexes to evidence this type of deformation which is otherwise invisible. Fig. 17 shows the associated profile and Fig. 18 presents the retrieved deformation fields for both central and diffuse deformation.

E. Robustness with Respect to the Approximative Center

For the deformation model, a very interesting feature of the spheres method is that it is not very sensitive to the precise location of the center P because once the sphere is larger than the lesion, the value ΔV_i is theoretically constant (but more and more noisy in practice). We have shifted the center P up to a three-voxels distance (for a lesion with a diameter of ten voxels) and measured the performance for the case of central
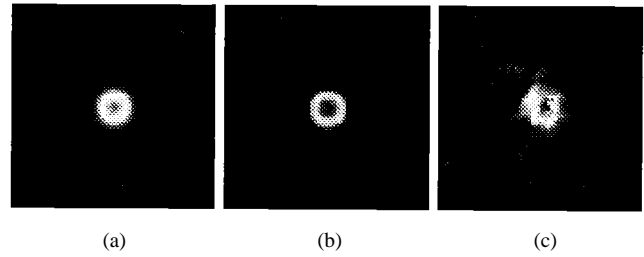

Fig. 18. $\|f\| \operatorname{div}(f)$ computed from the deformation fields. (a) Synthesized field. (b) Retrieved from central deformation images. (c) Retrieved from diffuse deformation images. Motion field analysis makes diffuse deformation clearly visible.

TABLE IV
ROBUSTNESS WITH RESPECT TO THE DISPLACEMENT d OF THE CENTER

Distance d (mm)	$\Delta(v)_{\mathrm{th}}$	$\Delta(v)_{\mathrm{sphere}}$
0.5	524	454
1	524	440
1.5	524	416
2	524	432
2.5	524	410
3	524	414

TABLE V
ROBUSTNESS WITH RESPECT TO SHAPE

R_x, R_y (mm)	R_z (mm)	$\Delta(v)_{\mathrm{th}}$	$\Delta(v)_{\mathrm{sphere}}$	$\Delta(v)_{\mathrm{iso}}$
4.368	6.552	524	393	451
3.969	7.937	524	402	484
3.684	9.210	524	343	469

deformation. The results are degraded progressively, but the volume-variation measurement is still valuable (see Table IV).

F. Robustness with Respect to Shape

It is not an easy task to derive the theoretical deformation field of complex shapes. We have performed experiments with only ellipsoidal lesions and for central deformation, with volume $V = 4/3\pi R_x R_y R_z$. In that case, the results are much better for the isosurface technique than for the spheres, as one would expect (see Table V).

G. Conclusion on Synthetic Experiments

Segmentation is probably best suited for pure tissue transformation, that is, when the tissues are not displaced. However, this model is unlikely to be realistic for actual lesions. When there is a deformation, we can have a continuous variation of cases in between central and diffuse deformation. For central deformation, our method relying on deformation field and a segmentation method can give comparable results. However, the deformation-field method becomes much better when the deformation is more important than the intensity changes. In that case, segmentation underestimates much more the volume variation than the deformation-field method, up to the point when segmentation cannot be used anymore (no visible intensity changes).

Again, segmentation is operating on single frames and is unable to detect tissue deformations. Hence, in real cases we can expect that if, for a given lesion, the volume variation
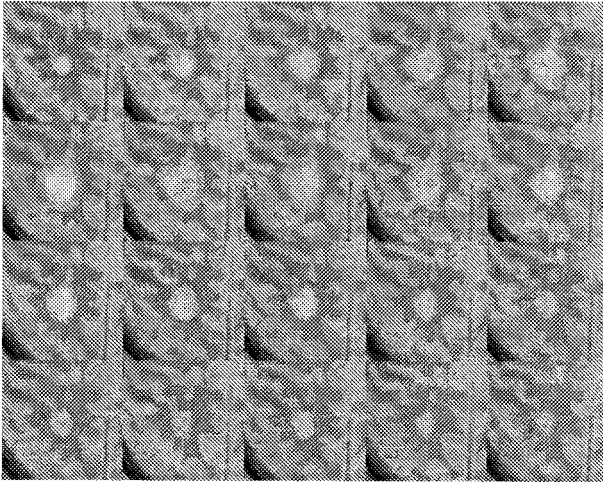
Fig. 19. The same ROI in the 20 successive images of the same patient (T2-weighted, first echo).

TABLE VI
MEASUREMENTS OF THE VOLUME VARIATION WITH A REAL PLAQUE (RESULTS IN mm^3), FOR THE TIME SERIES OF 20 VOLUMETRIC IMAGES, REPRESENTED IN FIG. 19

Image	1	2	3	4	5	6	7
ΔV_{seg}	738	876	674	593	356	40	-339
ΔV_{sph}	1451	1356	915	1114	1594	608	-895
ΔV_{iso}	1486	1415	1057	1175	1528	572	-837
Image	8	9	10	11	12	13	14
ΔV_{seg}	-499	-384	-387	-342	-312	-432	-174
ΔV_{sph}	-1792	-812	-1044	-617	-403	-455	-334
ΔV_{iso}	-1880	-1027	-1136	-738	-351	-583	-386
Image	15	16	17	18	19		
ΔV_{seg}	-308	69	-181	-143	-100		
ΔV_{sph}	-189	-319	-153	-162.5	-232		
ΔV_{iso}	-182	-87	-141	-183	-161		

obtained with the deformation-field analysis is significantly larger than the one measured by segmentation, this is evidence of a deformation of the tissues, or mass effect, larger than the visible spot which can be segmented.

VII. MEASUREMENTS ON REAL MULTIPLE SCLEROSIS IMAGES

A close inspection on real MS plaques reveals that, in addition to a clearly visible bright spot in the center, some lesions are surrounded by a cloudy halo whose intensity can hardly be distinguished from the surrounding white matter. This strongly suggests that MS plaques are in fact larger than their visible central spots.

Another clue for this hypothesis is provided by dynamic sequences of accurately registered volumetric images. We have registered the volumetric images of a time sequence of 24 time frames (courtesy of Dr. R. Kikinis and C. Guttmann, see Fig. 19) and we have been able to evidence visually a deformation of the surrounding tissues induced by the lesion. The gyri of the brain are pushed when the lesion is growing, and return to place when it is shrinking (growing and shrinking is a normal course for active plaques). What is surprising is that this displacement is visible, even quite far from the central spot (up to ten voxels). Because the deformation effect decreases in $1/r^2$ in 3-D, the central spot alone cannot explain visible displacement that far from the center. It can be sensitive only two or three voxels apart, and the only explanation that we found is that a diffuse deformation, much larger in extension than the visible spot, is responsible for these displacements of tissues.

To give quantitative grounds to this assumption, we have compared the volume variation obtained by segmenting the plaque visible in the 20 images of Fig. 19 with the results of the spheres and the isosurfaces method (see Table VI or Fig. 20). The variations obtained by the deformation-field methods are much larger (about two times) than the ones obtained by segmentation, which justifies our hypothesis. We can see also that the spheres and the isosurfaces methods give coherent results and that, as in synthetic cases, the isosurface variations are generally slightly larger. The profiles
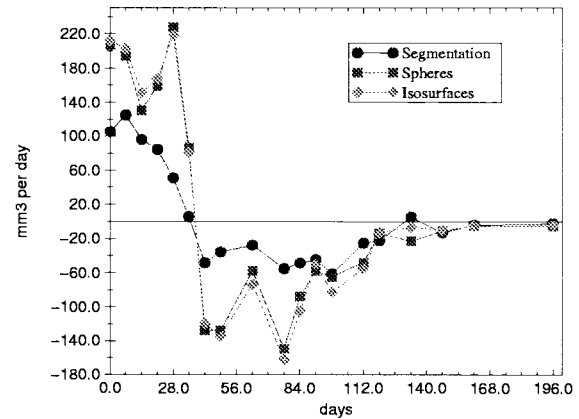

Fig. 20. Temporal volume variation (dV/dt) with a real plaque for the time series of 20 volumetric images (results in mm^3 per day): comparison of segmentation, spheres method, and isosurfaces method.
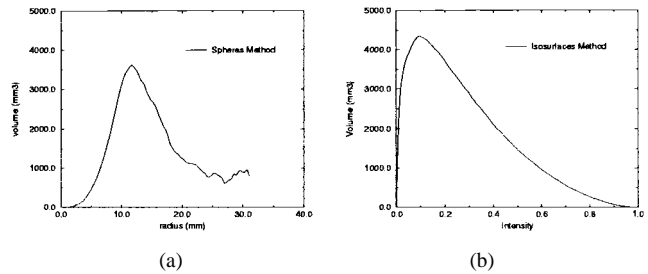

Fig. 21. Profile of ΔV_i for real images. (a) Measured with the spheres. (b) Measured with the isosurfaces (computed between frames one and four).

ΔV_i obtained in the real case are qualitatively similar to the theoretical ones (compare Figs. 14 and 21) which is an additional confirmation of the validity of our model. As the lesion is not spherical, we believe that the isosurfaces measurement method is the most reliable. In fact, even a volume variation twice as large as that measured by segmentation seems to us insufficient to fully explain the visual effect in the dynamic sequence. We saw previously that the isosurfaces method underestimates pure diffuse deformation in synthetic experiments (by about a factor of two), hence, we believe that the value which is provided by our method is a lower bound of an even larger diffuse deformation.

By integrating the volume variation (see Table VII or Fig. 22) we can estimate the absolute volume from both

TABLE VII
ESTIMATION OF THE VOLUME WITH A REAL PLAQUE (RESULTS IN mm^3), FOR A TIME SERIES OF 20 VOLUMETRIC IMAGES, REPRESENTED IN FIG. 19. NOTE THAT FOR THE DEFORMATION FIELD ANALYSIS TECHNIQUES (SPHERES AND ISOSURFACES), THIS VALUE IS OBTAINED BY INTEGRATION FROM THE FIRST VALUE GIVEN BY THE SEGMENTATION, HENCE IT CAN BE SUBJECT TO INCREASING ERRORS

Image	1	2	3	4	5	6	7
ΔV_{seg}	350	1088	1964	2638	3231	3587	3627
ΔV_{sph}	350	1801	3157	4072	5186	6780	7388
ΔV_{iso}	350	1836	3251	4308	5483	7011	7583
Image	8	9	10	11	12	13	14
ΔV_{seg}	3288	2789	2405	2018	1676	1364	932
ΔV_{sph}	6493	4701	3889	2845	2228	1825	1370
ΔV_{iso}	6746	4866	3839	2703	1965	1614	1031
Image	15	16	17	18	19	20	
ΔV_{seg}	758	450	519	338	195	95	
ΔV_{sph}	1036	847	528	375	212	-19	
ΔV_{iso}	645	463	376	235	52	-109	

Fig. 23. Temporal coherency and coherency with a change of MR sequence: volume-variation profiles (plaque of Fig. 2) obtained by segmentation, by relative measurements, and by absolute measurements (isosurfaces method). (a) Results obtained with T_2-weighted MR images. (b) Results obtained with proton density MR images.
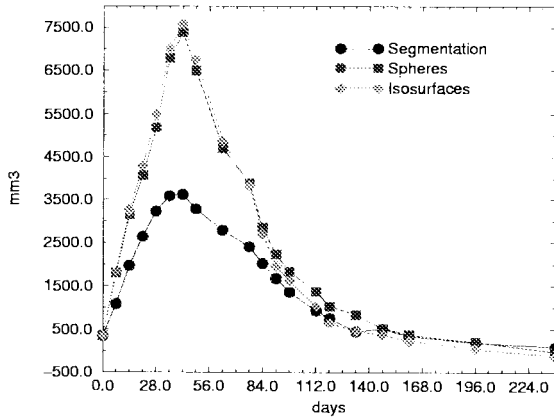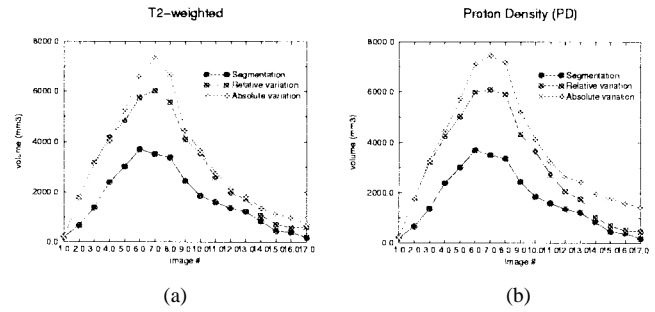

Fig. 22. Volume of a real plaque for the time series of 20 volumetric images: comparison of segmentation, spheres method, and isosurfaces method.

respect to temporal coherency, because the integration of the relative volume variations accumulates, in the end, the errors of 20 independent measurements and is still very close to the absolute measurements.

2) Coherency Between Different Echos: For the same patient and for each time frame we have both the T_2-weighted and the proton density volumetric images. An interesting experiment is to compare the computation performed independently in both types of images (T_2 and proton density). The result is also presented in Fig. 23. The results of segmentation, absolute variation measurements, and relative variation measurements are not very sensitive to the change of MR sequence, which suggests that the measures are intrinsic to the tissue displacements and relatively independent of image contrast.

B. Comparison with Deformations Obtained with Cross-Correlation

One possible drawback of the method that we are using to evaluate the deformation field is that, because it is relying on the optical flow paradigm (conservation of image intensity), it can be influenced by intensity changes. Global intensity changes are taken into account because global linear transformations between the intensities of the two successive images of the sequence are estimated (using linear regression between the joint intensity map) and compensated for.

However, local intensity changes also have an influence which cannot be easily discarded. To evaluate this effect, we have implemented an independent way to evaluate a dense deformation field between two images. The principle is to search, for a subwindow defined around each voxel (typically a 5 voxels^3 subwindow), a sub-window (of 5 voxels^3) in the second image which correlate the most with this one. This subwindow is searched in a larger window (typically 12 voxels^3) centered on the voxel having the same coordinate in the second image. It should be noted that this method works only for very small deformations and is highly time consuming. The following formula is the cross-correlation coefficient $c(\boldsymbol{x}, \boldsymbol{y})$ measured between two subwindows of n voxels where $\boldsymbol{x}$ are the intensities for locations in the first

the spheres and the isosurfaces measurements and compare it to segmented volumes. The volume profile obtained from the segmentation and from the deformation-field methods are very coherent except for a multiplicative factor, which suggests that the mass effect is present at each stage of the evolution.

A. Some Validation Experiments with Real Images

These data enable us to perform some useful validation experiments[2] and check for the coherency of the results.

1) Temporal Coherency: As we have 20 time frames, a first experiment consists in comparing the integration of the results obtained between times 1 and 2, times 2 and 3, ..., times $n - 1$ and n (relative volume variations, as in the previous section), with respect to the direct computation of the volume variation between times 1 and 2, times 1 and 3, ... times 1 and n(absolute variations). In Fig. 23 we compare the absolute and relative variations, which shows a difference of only a few percent. These are nice results with

[2]This does not replace other *in vitro* experiments and *in vivo* studies which are necessary for a complete medical validation, which is the subject of a collaboration that we have started with Dr. N. Roberts, University of Liverpool.
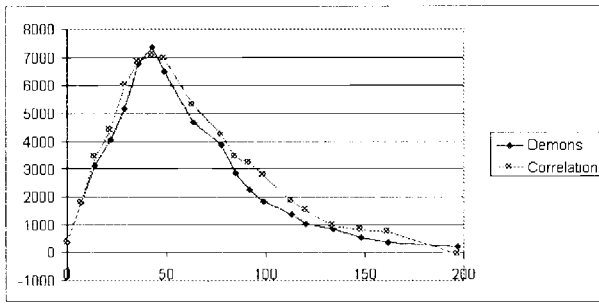
Fig. 24. Comparison between volume-variation profiles obtained using a method close to optical flow (demons) and a method based on cross correlation for a time sequence in the case of an MS plaque presenting a mass effect. This result shows independence of results with respect to the method used to evaluate the deformation field.

image and y intensities in the second image

$$C(x,y) = \frac{\sum_{i=1}^{n}(x_i - \overline{x})(y_j - \overline{y})}{\left(\left(\sum_{i=1}^{n}(x_i - \overline{x})\right)\left(\sum_{j=1}^{n}(y_j - \overline{y})\right)\right)^{1/2}} \quad (5)$$

where $\overline{x} = 1/n\ \Sigma_{i=1}^{n}\ x_i$ and $\overline{y} = 1/n\ \Sigma_{i=1}^{n}\ y_i$.

The principal advantage of cross correlation is that it is insensitive to local intensity variations (when the spatial extension of these variations is larger than the subwindow size). The principal drawback of cross correlation is computation time. Our implementation of cross correlation is 50 times slower than the implementation relying on optical flow.

The results are qualitatively very similar between both deformation measurement methods (see Fig. 24). This result shows some independence with respect to the method used to evaluate the deformation field and confirm our hypothesis of mass effect for some MS plaques.

C. Grounds for a Mass Effect for MS

The coherence of the results between real experiments and also with respect to synthetic experiments increase our confidence in our quantification of mass effects. We believe now that some MS plaques are subject to a mass effect of at least twice the volume of the visible plaque. Of course, we do not demonstrate that there is a mass effect for every plaque in MS. We now have a method to determine which plaque is active or inactive and, if active, whether it is subject to a mass effect. Such measurements open up new ways to evaluate the impact of drug treatments for this particular disease.

VIII. CONCLUSION

Thanks to a highly accurate 3-D registration algorithm and time sequences of volumetric images, we had visually observed in some patients' T2 MR images a diffuse deformation or mass effect in the case of MS (the eye being a precious tool to perform optical flow analysis). To our knowledge, the present paper is the first attempt to quantify a mass effect *in vivo* for MS. To achieve this, we have developed

an original method to compute volume variations based on the integration of the deformation fields obtained between different time frames. The volume-variation profiles obtained from the segmentation and from deformation-field integration are very coherent except for a multiplicative factor, which suggests that the mass effect is present at each stage of the evolution and that it is at least twice as large as the visible plaque evolution. This applies to the studied cases, however, more experiments have to be made to determine the proportion of the MS diseased population which is presenting this kind of phenomenon (the cases that we have studied are presenting especially large plaques). This first result is extremely promising to better understand the disease. Our detection and quantification methods can help also to quantify more precisely the impacts of new drugs (such as β Interferon) which are now tested in many ongoing clinical trials. The application of our tool, however, is not limited to MS plaques, but can be applied to the study of other pathologies such as cancer tumors.

REFERENCES

[1] H. G. Barrow, J. M. Tenenbaum, R. C. Bolles, and H. C. Wolf, "Parametric correspondence and chamfer matching: Two new techniques for image matching," in *Proc. 5th Int. Joint Conf. Artificial Intelligence*, Cambridge, MA, 1977, pp. 659–663.

[2] D. J. Burr, "A dynamic model for image registration," *Comput. Graph. Image Processing*, vol. 15, no. 2, pp. 102–112, Feb. 1981.

[3] I. Cohen, L. Cohen, and N. Ayache, "Using deformable surfaces to segment {3D} images and infer differential structures," in *Proc. CVGIP: Image Understanding '92*, Sept. 1992.

[4] H. E. Cline, W. E. Lorensen, R. Kikinis, and F. Jolesz, "Three-dimensional segmentation of mr images of the head using probability and connectivity," *JCAT*, vol. 14, no. 6, pp. 1037–1045, 1990.

[5] G. C. Cruywagen, D. E. Woodward, P. Tracqui, G. T. Bartoo, J. D. Murray, and E. C. Alvord, "The modeling of diffusive tumours," *J. Biol. Syst.*, vol. 3, no. 4, pp. 937–945, 1995.

[6] H. Demiray, "Large deformation analysis of some soft biological tissue," *J. Biomechan. Eng.*, vol. 103, pp. 73–78, May 1981.

[7] G. Gerig, W. Kuoni, R. Kikinis, and O. Kübler, *Medical Image and Computer Vision: An Integrated Approach for Diagnosis and Planning.* Berlin, Germany: Springer-Verlag, 1989, pp. 425–443.

[8] G. Gerig, D. Welti, C. Guttmann, A. Colchester, and G. Székely, "Exploring the discrimination power of the time domain for segmentation and characterization of lesions in serial mr data," in *Proc. Medical Image Computing and Computer-Assisted Intervention—MICCAI'98*, Oct. 1998, pp. 469–479.

[9] S. K. Kyriacou and C. Davatzikos, "A biomechanical model of soft tissue deformation, with applications to nonrigid registration of brain images with tumor pathology," in *Proc. Medical Image Computing and Computer-Assisted Intervention—MICCAI'98*, Oct. 1998, pp. 531–538.

[10] R. Kikinis, C. Guttmann, D. Medcalf, W. Wells, G. Ettinger, H. Weiner, and F. Jolesz, "Quantitative follow-up of patients with multiple sclerosis using MRI part I: Technical aspects," Surgical Planning Lab., Brigham and Women's Hosp., Harvard Med. School, Boston, MA, Tech. Rep. 39, Oct. 1996.

[11] M. Kass, A. Witkin, and D. Terzopoulos, "Snakes: Active contour models," *Int. J. Comput. Vision*, vol. 1, pp. 312–331, 1987.

[12] D. Medcalf, R. Kikinis, C. Guttmann, L. Vaina, and F. Jolesz, "4d connected component labeling applied to quantitative analysis of ms

lesion temporal development," in *Proc IEEE EMBS Conf.*, Paris, France, Oct. 1992.

[13] X. Pennec and J. P. Thirion, "Validation of 3-d registration methods based on points and frames," in *Proc. 5th Int. Conf Comp. Vision (ICCV95)*, Cambridge, MA, June 1995, pp. 557–562.

[14] N. Roberts, S. Barbosa, L. D. Blumhardt, R. A. Kowaski, and R. H. T. Edwards, "Stereological estimation of the total volume of mr visible brain lesions in patients with multiple sclerosis," *MAGMA*, vol. 2, pp. 375–378, 1994.

[15] S. A. Roll, A. C. F. Colchester, L. D. Griffin, P. E. Summers, F. Bello, B. Sharrack, and D. Leibfritz, "Volume estimation of synthetic multiple sclerosis lesions: An evaluation of methods," in *Proc. 3rd Ann. Meeting Society Magnetic Resonance*, Nice, France, Aug. 1994, p. 120.

[16] C. Roszmanith, H. Handels, S. J. Pöppl, E. Rinast, and H. D. Weiss, "Characterization and classification of brain tumours in three-dimensional mr image sequences," in *Proc. Visualization Biomedical Computing, VBC'96*, Hamburg, Germany, Sept. 1996.

[17] J.-P. Thirion, "Software to assist in monitoring treatment," in *Proc. IBC's 3rd Ann. Multiple Sclerosis Conf.*, Boston, MA, May 1995.

[18] _____, "New feature points based on geometric invariants for 3D image registration," *Int. J. Computer Vision*, vol. 18, no. 2, pp. 121–137, May 1996.

[19] _____, "Image matching as a diffusion process: an analogy with Maxwell's demons," *J. Med. Image Anal.*, vol. 2, no. 3, pp. 243–260, 1998.

[20] C. J. Wallace, T. P. Seland, and T. C. Fong, "Multiple sclerosis: The impact of MR imaging," *AJR*, vol. 158, pp. 849–857, Apr. 1992.

[21] J. S. Young, "The invasive growth of malignant tumours: An experimental interpretation based on elastic-jelly models," *J. Pathol. Bacteriol.*, vol. 77, no. 2, pp. 321–339, 1959.